JOURNAL OF MATERIALS SCIENCE 29 (1994) 5529–5540

Nanoindentation studies of the chemomechanical effect in sapphire

S. V. HAINSWORTH, T. F. PAGE
Materials Division, Department of Mechanical, Materials and Manufacturing Engineering, University of Newcastle, Newcastle upon Tyne NE1 7RU, UK

For the first time, nanoindentation techniques have been used to study chemomechanical effects due to water, alcohols and myristic acid on the detailed surface mechanical response (e.g. elastic flexure, stiffness, dislocation nucleation and plasticity) of $(10\bar{1}2)$ single-crystal sapphire. Because the magnitude of surface tension forces at these small scales can be comparable with the applied load, the experiments have been performed on samples annealed, quenched into various environments and tested after the liquid had been allowed to evaporate. At low loads and indentor displacements (i.e. $\leqslant 60$ nm), two separate effects have been identified: the occurrence of a soft surface layer together with significant differences in the elastic–plastic deformation transition. The experiments were repeated after a 4 week exposure to ambient laboratory atmosphere and in each case, the behaviour had moved towards that displayed by the original water-quenched sample. The results are explained in terms of physisorption and chemisorption on dislocation nucleation behaviour and subsequent plasticity. At higher loads, the results showed that the previously conflicting evidence from microhardness testing concerning these effects is not surprising, because no differences in the load–displacement responses were seen. However, scanning electron microscopy of the indentations showed significant differences in the deformation behaviour. Low-load creep experiments were also performed but, in contrast to reported microhardness responses, showed no real evidence for time-dependent deformation behaviour. The results presented clearly show the advantages and potential of nanoindentation techniques for investigating these effects.

1. Introduction

Generically, ceramics possess high hardness, good chemical stability and high specific stiffnesses which are maintained to high temperatures. These properties make them attractive for wear-resistant components and surface coatings in demanding conditions. However, there are many instances where friction and wear behaviour has been found to be influenced by the environment in which components operate. This can be because of simple chemisorbtion affecting adhesive friction (e.g. [1]) and/or because the environment changes the dominant wear mechanism and/or because the near surface mechanical properties of the material itself are genuinely environmentally sensitive. The effects of environment on wear are well established and usually involve chemical reaction-rate controlled wear in which either oxide or water-softened layers are continually removed from carbides, nitrides and oxides (e.g. [2–4]). However, while environmental effects on fracture and slow crack growth are well established (e.g. [5]), attempts to conclusively demonstrate that the plasticity of ceramics- and thus their indentation hardness (the so-called Rebinder of chemomechanical effects) is sensitive to the operating environment have been far less convincing (e.g. [6–9]). The principal reason is that the possible magnitude of the variously reported changes in hardness is only of the order of typical experimental errors encountered in low-load (~ 0.01–1 N) microhardness testing which has previously been the most widely used experimental technique for exploring such near-surface phenomena. Further, the proposed mechanisms controlling any such effects are not well understood. Possibilities have included simple physisorption and chemisorption (e.g. particularly of water) altering indentor–specimen friction (e.g. [9]) and more complex effects whereby physisorbed or chemisorbed layers affect near-surface dislocation mechanisms by altering the local electronic band structure (which influences the rate of bond break–make in the dislocation core, (e.g. [8, 10]). Sometimes these effects have been described as showing a variation with zeta potential (e.g. [9]) whilst other workers have speculated on the effects of proton tunnelling from the absorbed species into the solid [11]. In many cases, changes in the time-dependent deformation behaviour, or anomalous indentation creep, during indentation tests at low homologous temperatures have been widely reported in microhardness tests on ceramics exposed to various environments (e.g. [12–14]) under conditions where clean, dry samples show no similar progressive deformation. To add to the confusion, the response

0022–2461

may be specific to individual environments to the extent that differing hardness values have been reported for ceramics tested in each of a homologous series of alcohols (e.g. [15]). Whatever the detailed causes, such phenomena have been reported to cause either changes in local hardness and/or changes on the balance of plasticity and fracture effects occurring in response to surface contact during machining, wear and scratching experiments, etc. Thus, future advances in either our understanding or exploitation of such chemomechanical effects (e.g. in aiding precision machining of ceramics) require investigative techniques capable of identifying the changes in mechanical response in a far less ambiguous manner.

One key experimental problem has been that even low-load microhardness techniques probe mechanical properties over depths that are large compared with any very near-surface, environmentally (or electronically) affected layer. For example, a 0.1 N Vickers indentation in sapphire is ~ 1 μm deep whilst a comparable Knoop indentation still penetrates ~ 0.25 μm. However, recently there has been considerable interest in the development and application of nanoindentation techniques. These micromechanical test methods generally provide a continuously recorded load–displacement plot for ultra-low-load indentation experiments with typical load and displacement resolutions of $\pm$ 0.08 μN and $\pm$ 0.04 nm (e.g. [16, 17]). Thus this method can readily be used to characterize the elastic flexure response of surfaces to very low-load contact experiments, to investigate the elastic–plastic transition (sometimes witnessed by sharp discontinuities in displacements ("pop-in") at some critical load as dislocations are nucleated) and to characterize subsequent plasticity-controlled indentation behaviour (e.g. [18–20]). A further attraction is that by producing continuous load–depth–stiffness–time data, the technique removes many of the ambiguities and problems associated with the *post facto* measurement of indentations usually employed in microhardness testing and thus allows a more complete assessment of the mechanical response to be established. Not only does this minimize the effect of operator subjectivity in making measurements (which are often near the resolving power limit of light optics) but it also allows differences in elastic and plastic responses to be separated. For example, Fig. 1a shows schematic load–displacement curves for three hypothetical materials which have similar plastic responses (shown by the residual indentor displacement, δ_R, and the plastic work of indentation, W, as detailed in Fig. 1b) and therefore identical conventional hardness values: however, they display widely different amounts of elastic flexure (resulting in different values of the indentor displacement at maximum load, δ_{max}, and the proportion of elastic recovery occurring on unloading, $\%R$ (defined here as $[(\delta_{max} - \delta_R)/\delta_{max} \times 100]$). Thus, in this case, hardness values alone do not fully differentiate the characteristic mechanical responses of each sample and a more complete analysis of the nanoindentor load–displacement plot is required [21]. Further, the load–displacement plots themselves have to be assessed for phenomena such as pop-ins' which often result from deformation transitions (e.g. [19]). Another advantage of nanoindentation is that the stiffness of the indentor–specimen contact can be continuously measured and, if the tip-end geometry is accurately calibrated, elastic modulus values can be obtained for the small sample volume under investigation. The continuous load–displacement–stiffness–time record also allows a detailed investigation of creep effects (e.g. [22, 23]). Nanoindentation methods thus seem ideally suited for probing the detailed origins of chemomechanical effects, especially because changes in mechanical properties may be restricted to a layer only a few nanometres in thickness. However, while the load and depth sensitivity of nanoindentation makes it an attractive technique for such studies, it also places restrictions on the type of experiment that can be performed. Essentially it is difficult to carry out well-controlled nanoindentation experiments on surfaces either immersed in liquids or covered with discrete liquid droplets. This is primarily because

(i) the surface tension forces on the tip can be of the order of the loads required to examine very near-surface properties (this would also apply even if the indentor shank were immersed to a considerable depth, e.g. in a deep well);

(ii) the expected change in contact stiffness experienced as the indentor cuts through any liquid meniscus

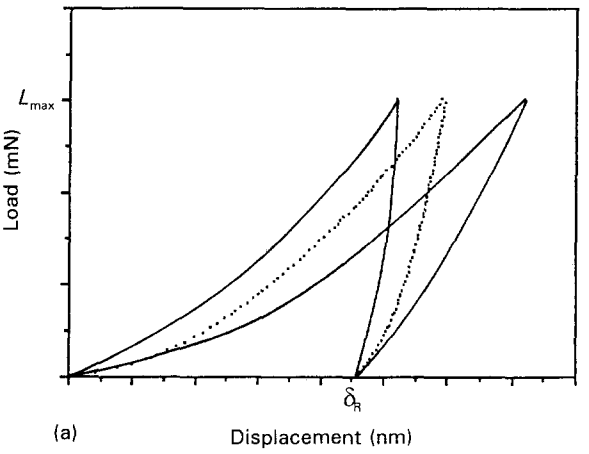

Figure 1 (a) Schematic load–displacement curves for three hypothetical materials displaying the same amount of plastic deformation (i.e. residual displacement, δ_R) but with differing elastic contributions (i.e. different values of δ_{max}) when tested to the same maximum load, L_{max}. The conventional hardness values of these three materials (calculated from δ_R) would be the same despite their different load–displacement histories and therefore mechanical properties. (b) A typical load–displacement curve for a substrate exhibiting mixed elastic–plastic behaviour. The sense of loading and unloading is shown by the arrow. The parameters listed on the right-hand side can all be readily obtained from this curve: L_{max}, is the maximum load needed to achieve the maximum displacement; δ_L, the maximum displacement; δ_R, the residual displacement after elastic recovery on unloading; $\%R$, the percentage elastic recovery (i.e. $[(\delta_{max} - \delta_R)/\delta_{max} \times 100]$; H_L a load-on hardness value calculated from δ_{max}; H_R, a conventional load-off hardness value based on the residual indentation depth, δ_R; W is the total irreversible work dissipated during indentation, and S is the contact stiffness. S can be used to calculate the elastic modulus of the surface if the tip-end geometry has been accurately established.

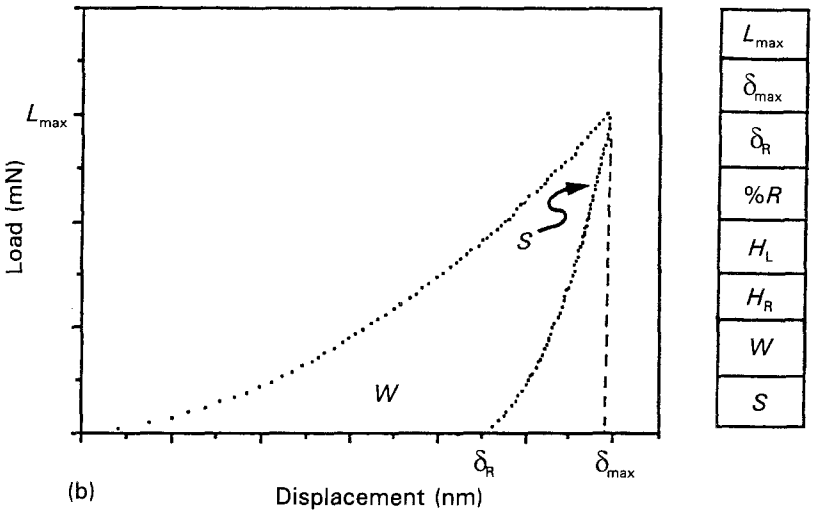

Figure 1 (Continued) (b)

is likely to lead to errors in locating the ceramic surface (which is detected as an increase in stiffness) [24].

This paper reports our first attempts to use nanoindentation to explore the possible effects of environment on annealed surfaces of single-crystal ($10\bar{1}2$) sapphire that have been exposed to various environments and then allowed to dry. Whilst this is not ideally comparable to previously reported techniques, it does establish that nanoindentation is capable of allowing some of the subtle effects controlled by environmental sensitivity to be distinguished and quantified.

2. Experimental procedure

Ultra-low-load indentation (nanoindentation) experiments were carried out using a Nano Indentor™ II mechanical properties microprobe (Nano Instruments Inc, Knoxville, TN, USA).

Several single-crystal ($10\bar{1}2$) sapphire wafers were cleaned and degreased with 1, 1, 1 trichloroethane and then heat treated in air at 500 °C for 6 h to remove any residual physisorbed or chemisorbed water or solvents. The device-grade wafers (courtesy GEC, Wembley, UK) had been pre-polished to a good optically flat finish and cleaved into $\sim 5\,mm \times 10\,mm$ samples prior to annealing. One set of samples were cooled in air ("normalized") as a control and the others were quenched from the furnace into a variety of solvents previously reported to induce chemomechanical effects in sapphire [6, 7, 9, 12–15]. The solvents used were methanol, ethanol, distilled and deionized water and myristic acid dissolved in paraffin oil to saturation. Fresh dry methanol was also used to try and eliminate any effects from the presence of water in the solvent. Once the samples had been quenched into the environment they were allowed to equilibrate for approximately 10 min before being removed and the residual liquid traces left to evaporate. No obvious residues were left on the sample surfaces. All the samples were then firmly affixed to aluminium nanoindentor specimen mounts with a high-purity thermoplastic wax which melted at approximately 60 °C. Care was taken not to overheat the stubs so that the temperature was kept as low as possible. Also, each sample was mounted in the nanoindentor stage to maintain, as near as possible, the same azimuthal orientation to the indenter and thus minimize any effects due to crystallographic anisotropy (e.g. [19]).

Indentations were then made as soon as possible after mounting, but a delay of at least 12 h had to be allowed for the specimens to equilibrate thermally within the thermally lagged nanoindentor cabinet. This was to eliminate as much thermal drift in the displacement data as possible (typical measured experimental drift rates were less than $0.03\,nm\,s^{-1}$). An array of 20 trigonal Berkovich indentations was then made, ten at each of two indentation depths (nominally 30 and 50 nm), to examine very shallow penetration behaviour and to be in the range where the applied load on the indentor first nucleates dislocations in sapphire [19]. Some cracking of the samples was observed (from the quench) and in all cases care was taken to locate the indentation arrays well away from cracks and microcracks. The indentations were made to a set displacement depth in order to compare like volumes of deformed material. The load range required to produce these depths was 1–4 mN. All the indentation experiments were performed using a loading rate of $15\,\mu N\,s^{-1}$ and with a hold segment on unloading at 70% of peak load to measure the thermal drift of the instrument. The raw load–displacement data were then processed using proprietary software to produce load–displacement plots corrected for thermal drift and machine constants (e.g. load frame compliance). A second set of identical experiments was carried out 4 weeks later (on the same samples still locked into the nanoindentor stage) to investigate any effects of prolonged exposure to the ambient laboratory atmosphere.

Further sets of indentations were carried out on the normalized and water-quenched samples to 20, 40, 60, 80 and 100 mN to determine if any effects could be seen at higher loads (comparable to the microhardness range). A set of experiments were also performed on these two samples with a hold period at peak load (of 1 mN) to investigate any time-dependent deformation (creep) behaviour.

Indentations were imaged using a CamScan S4-80DV scanning electron microscope (SEM) equipped with a high brightness LaB_6 source using a liquid-nitrogen cold trap to minimize contamination rates. An accelerating voltage of 15 kV was used in order to obtain a compromise between image resolution, gun brightness and beam penetration. Although microstructural observations are no longer necessary for estimating the size of the indentations, they are invaluable for characterizing deformation behaviour (e.g. [19, 24]).

3. Results

The results of the nanoindentation experiments show distinct differences for different environments. Some of the differences are immediately obvious by comparing the shape of the individual load–displacement curves, while other more detailed effects are only apparent on statistical analysis of the data. Thus the results are presented in two ways; load–displacement curves which show the different types of response that were seen, and tables which show the values of a number of parameters averaged for all the indentations in a particular load/environment combination.

3.1. Low-load experiments

Fig. 2 shows the two types of curve that were commonly seen for the shallower penetration depth of ~ 30 nm. Fig. 2a shows a "perfectly elastic" indentation in which, on unloading, almost complete recovery of the indenter displacement was observed. At low loads ($\ll 0.1$ mN), there is an initial flat portion of the curve which is consistent with the indenter contacting and penetrating a soft surface layer (e.g. [21]). The remainder of the response is elastic and this type of curve is described as "elastic" in the tables which follow. This behaviour was mainly seen for the samples quenched into alcohol environments and particularly for those samples quenched into methanol. Fig. 2b shows a second type of curve that was seen mainly for the water-quenched and normalized samples. In this case, there is a residual displacement of the indentor made up of the initial displacement in the soft surface layer and also a residual plastic displacement in the "substrate". Thus, while a large amount of elastic recovery is still evident ($\%R$), the finite area between the loading and unloading curves reveals significant plastic work, W, during indentation.

Fig. 3 shows the types of curves that were seen for the larger indentor displacement of ~ 50 nm. Results for this indentation depth were much more varied with two general types of response, mixed elastic–plastic behaviour with no evidence of "pop-in" (e.g. Fig. 3a, which is essentially similar to Fig. 2b but extended to a larger displacement) and those which showed pop-in (e.g. Fig. 3b and c). Pop-in is a sudden displacement discontinuity in an otherwise smooth load–displacement curve which, at this load range in sapphire, usually marks the onset of plasticity by the nucleation of dislocation loops [19]. Fig. 3b shows a curve with a "big" pop-in as opposed to the smaller

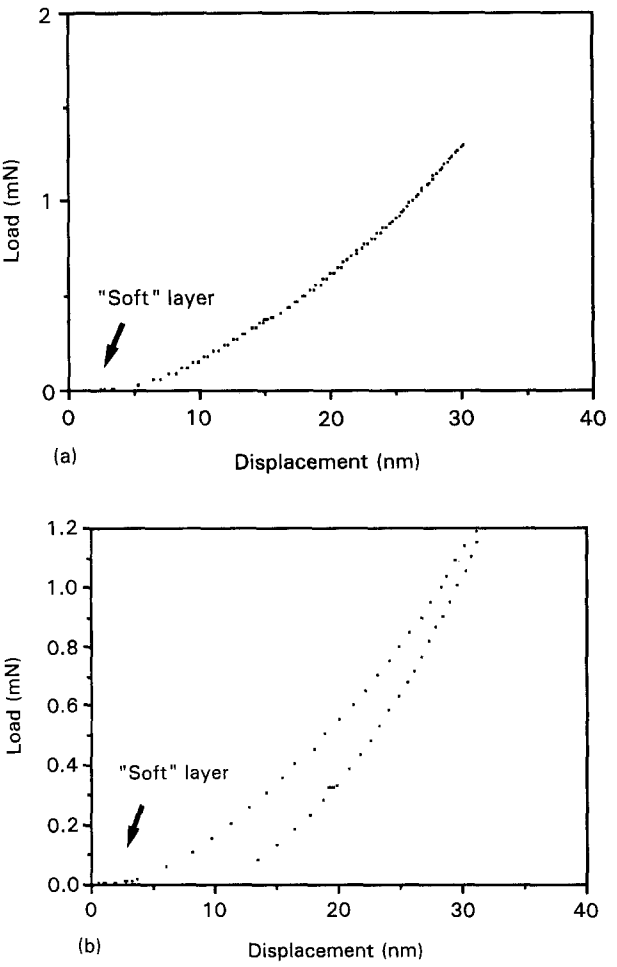

Figure 2 Typical examples of the load–displacement responses at small (~ 30 nm) indentor displacements (see also Table I). (a) A wholly elastic response whereby the indentor displacement is exactly retraced upon unloading. The first ~ 5 nm of the displacement has a lower stiffness than the rest and is attributed to the indentor penetrating a "soft" surface layer presumed to be associated with water absorption (see text). (b) A typical response with mixed elastic–plastic behaviour; while a significant amount of elastic recovery occurs on unloading but there is also some residual plastic deformation (i.e. a significant work of indentation has occurred). However, unlike Fig. 3b, there is no obvious critical load for the nucleation of dislocations (i.e. no pop-in behaviour).

multiple pop-ins of Fig. 3c. The "big" pop-ins were characteristically seen in the alcohol-quenched samples on the first set of experiments whereas the smaller multiple pop-ins were seen after 4 weeks. Several other types of curve were seen. For example, Fig. 3d shows pop-in occurring on unloading, while Fig. 3e and f show a reverse pop-in or "pop-out", a discontinuity in the unloading curve due to the sample exerting a sudden upthrust on the indentor. These only occurred in samples exposed to water (either on quenching or after 4 weeks). Possible causes are discussed later.

Table I shows results for the indentations to 30 nm while Table II shows results for the 50 nm indentations. The tables show that there are recognizably different effects on the plasticity behaviour of the samples from the different environments. There are differences in the number of totally elastic indentations, the number of pop-ins that occur, the loads at which pop-in occurs, the size of the pop-ins and the residual displacements. In some cases there are two or

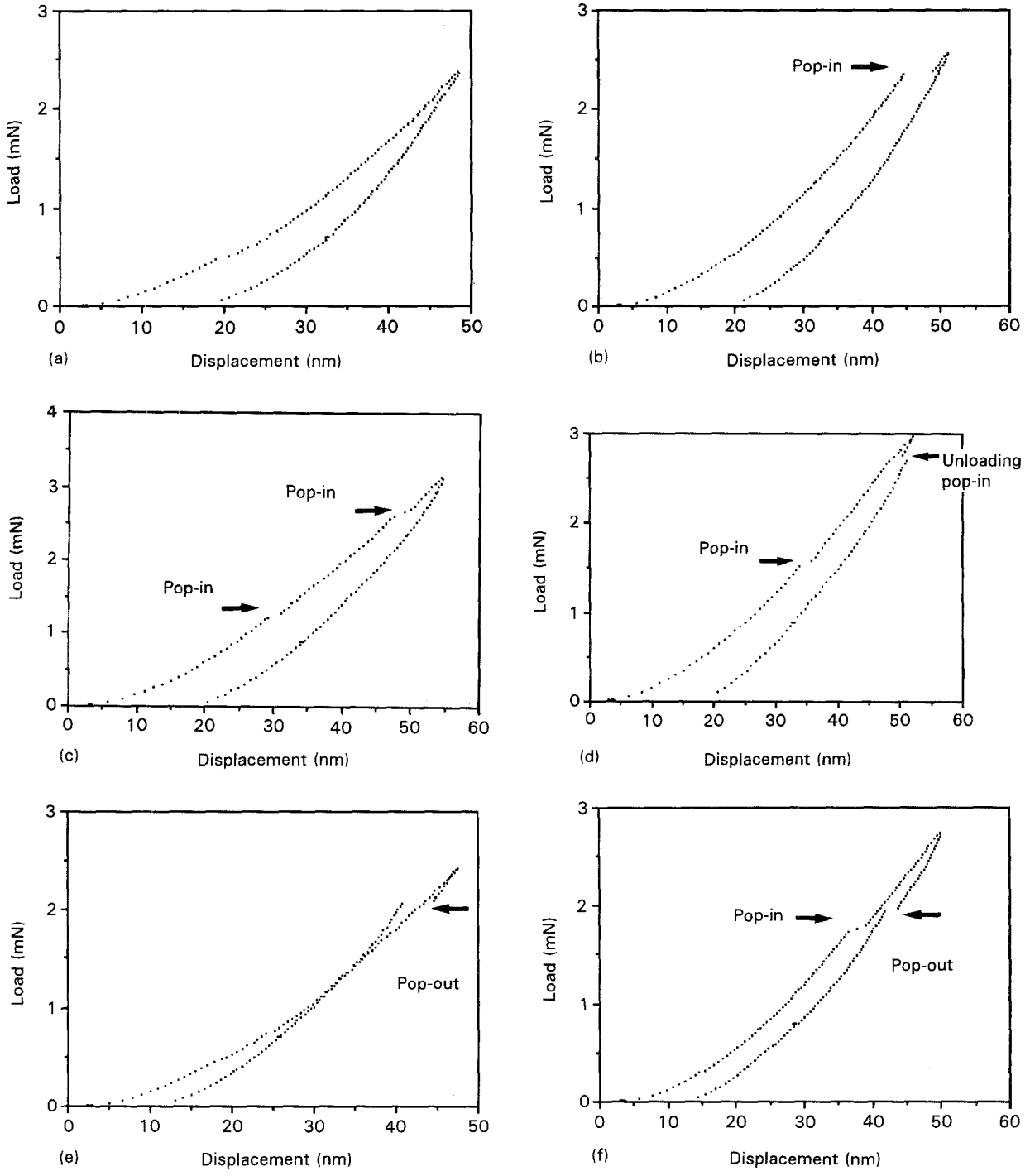

Figure 3 Typical examples of the 50 nm displacement behaviour (see also Table II). In most cases, pop-in behaviour (i.e. a sudden displacement discontinuity) occurs which is associated with dislocation nucleation in sapphire at these loads (see text). (a) Similar to Fig. 2b, showing significant plastic deformation with no discrete nucleation events. (b) Dislocation pop-in at a load slightly larger than that causing the wholly elastic response of Fig. 2a. The magnitude of the pop-in displacement is related to the sum of the Burgers vectors produced. (c) Progressive pop-ins at increasing loads. (d) Pop-in on initial unloading (reflecting the statistical nature and time-dependence of dislocation nucleation); (e, f) Pop-out on unloading, whereby displacements are suddenly recovered (e.g. by dislocation loop collapse) (see text).

more pop-ins for each indentation, pop-ins on unloading and pop-outs. Further, the tables show significant differences in the initial behaviour and that determined 4 weeks later.

For the 30 nm indentations, the normalized sample required the highest load to achieve the set displacement followed by the methanol and ethanol samples (which required similar loads), the distilled and deionized water and then the myristic acid and dry methanol (also similar loads). In all cases, the curves showed the effect of cutting through a soft surface layer of between 4 and 6 nm depth. "Elastic" curves showed this initial displacement but with a subsequent wholly elastic response from the "substrate". However, for all the samples, the majority of the indentations showed some residual displacement of both this soft surface layer and the "substrate". The methanol and ethanol samples showed the least residual displacement (i.e. the highest $\%R$).

For the 50 nm indentations, the pop-in behaviour from the different environments also showed distinct differences. Nearly all the methanol and ethanol

TABLE I Results for the 30 nm displacement experiments showing several of the parameters detailed in Fig. 1b each averaged ten indentations for each set of quench conditions. (However, parameters such as $\%R$ could only be averaged over those indentations not showing wholly elastic behaviour, etc.; pop-in behaviour is only averaged for those indentations showing pop-in, etc.). For each quench environment results are shown for initial experiments and for identical experiments performed after 4 weeks exposure to ambient laboratory atmosphere. By showing the load required to achieve the set indentor displacement, L_{max} reflects the overall (elastic + plastic) penetration resistance at this scale with the normalized sample being the most penetration resistant (despite the slightly larger indentor displacement achieved). However, the following columns reveal very significant differences in behaviour. Several samples show the wholly elastic response of Fig. 2a while only 12 pop-ins occurred (see Fig. 3b) over the 100 indentations. Significant differences in the amount of elastic recovery ($\%R$) also occur revealing differences in the balance of elastic and plastic responses – the greatest value (78%–80% displacement recovery) being for the ethanol and methanol quenches (i.e. least plasticity) with all values tending towards the water quenched value (70% ± 2%) after 4 weeks

Environment	L_{max} (mN)	δ_{max} (nm)	δ_R (nm)	$\%R$	Wholly elastic	Pop-in, (No., L_{crit}, δ_{crit})
Normalized	1.46	34.7	10.5	69.8	–	–
After 4 weeks	1.24	32.3	10.7	66.8	–	–
Distilled/deionized water	1.11	30.3	9.7	67.8	–	1, 0.82 mN, 1.0 nm
After 4 weeks	1.12	30.9	9.6	68.9	–	–
Methanol	1.29	31.1	6.0	80.7	5	–
After 4 weeks	1.28	31.4	9.3	70.5	2	4, 1.2 mN, 1.4 nm
Ethanol	1.29	31.8	6.9	78.3	1	–
After 4 weeks	1.49	33.2	9.2	72.3	1	6, 1.2 mN, 1.7 nm
Dry methanol	1.01	33.4	13.8	59.0	–	–
Myristic acid	1.06	33.6	13.8	58.6	–	1, 0.7 mN, 2.6 nm

TABLE II Results for the 50 nm indentation experiments. No indentations showed wholly elastic deformation at this displacement. As with the shallower displacement results in Table I, the normalized sample appeared the most penetration resistant (highest L_{max}) with a notable decrease after 4 weeks exposure to the ambient laboratory atmosphere. At this displacement, discrete pop-ins were widely observed with several pop-outs on unloading (see text). Multiple pop-ins on one loading curve are denoted by *. The values of $\%R$ are lower than for Table I showing that a larger proportion of plastic deformation is involved at this displacement

Environment	L_{max} (mN)	δ_{max} (nm)	δ_R (nm)	$\%R$	Pop-in, (No., L_{crit}, δ_{crit})	Other
Normalized	3.24	59.49	24.33	59.11	1, 2.7 mN, 2.0 nm	–
After 4 weeks	2.61	53.08	21.30	59.87	3, 1.4 mN, 1.4 nm	–
Distilled/deionized water	2.40	47.51	14.60	69.33	2, 0.5 mN, 1.6 nm	1 pop-out
After 4 weeks	2.46	49.80	18.50	62.90	–	–
Methanol	2.74	51.20	15.90	69.00	7, 2.4 mN, 4.0 nm	–
After 4 weeks	2.81	52.20	18.30	64.94	13*, 1.88 mN, 1.7 nm	1 unloading pop, 1 pop-out
Ethanol	2.62	50.71	17.40	65.70	8, 2.1 mN, 3.0 nm	–
After 4 weeks	3.07	54.91	20.80	62.10	17*, 2.0 mN, 1.8 nm	–
Dry methanol	2.54	54.98	24.30	55.80	3, 2.3 mN, 2.6 nm	–
Myristic acid	2.51	54.56	24.00	56.01	4, 1.8 mN, 2.2 nm	–

quenched samples showed pop-in. The pop-in displacements were quite large, ~3–4 nm. The other environments showed smaller (~1–2 nm) and fewer pop-ins. The methanol and fresh dry methanol samples were also significantly different, in that the methanol sample was more penetration resistant (as measured by the value of L_{max} required to reach the set displacement) than the fresh dry methanol environment. This shows that any dissolved water in the methanol used for the quench was not causing the major "softening" effect and that dry methanol alone has a larger chemomechanical effect than methanol combined with water.

3.2. Effect of exposure to the ambient environment

After 4 weeks, there were significant differences in the results from experiments identical to those performed initially on four specimens that had remained in the nanoindentor in exactly the same orientation so that the changes cannot be attributed to any differences in the experimentation. Unfortunately, it was not possible to leave all specimens mounted in the machine for this length of time and so there are no second set of results for the myristic acid and dry methanol samples. However, the results for the other four samples show some interesting trends. The loads required to produce the deformation in the normalized sample had now considerably decreased to almost the same as those for the initial distilled and deionized water sample. The loads required for the samples quenched into methanol were approximately the same but the loads required for the ethanol sample were greater (now approximately the same as those initially required for the normalized sample). The number and size of pop-ins had now also increased for all samples except the distilled and deionized water sample.

The changes in the results over the 4 week period suggests that there is an effect whereby the initial near-surface properties are altered. The results for the normalized sample after 4 weeks are very similar to those for the distilled and deionized water sample. This could be due to the normalized sample absorbing water from the atmosphere. The increases in the penetration resistance of the methanol and ethanol samples are more difficult to explain and are probably controlled by more complex phenomena than simple adsorption of water. Possible explanations include desorption of whatever species was originally absorbed and/or changes in the balance of adsorbates with time. The chemistry of the adsorption mechanisms is complex and identification of the adsorbates requires a combination of techniques and facilities beyond the present study.

3.3. Higher load experiments

A typical load–displacement curve for a higher load indentation is shown in Fig. 4. The load–displacement curves for both of the samples indented at higher loads had the same appearance. The data for both the normalized and water-quenched samples were analysed and no significant differences were detectable. These experiments demonstrate that it is not surprising that microhardness experiments have often shown conflicting evidence for the chemomechanical effect.

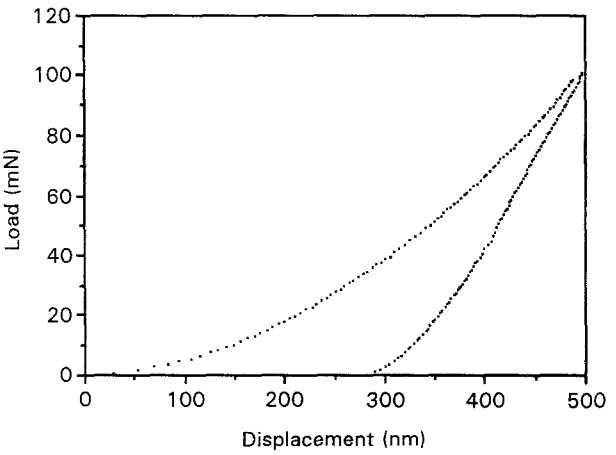

Figure 4 The load–displacement response for an indentation at 100 mN peak load, i.e. comparable with the lower end (~10 gf) of the microhardness scale. A smooth curve is seen, which at this scale displays none of the detail shown in the first few milliNewtons associated with soft surface layers and dislocation-nucleation events. Curves of this type showed no significant differences between environments.

3.4. SEM observations

Indentations with residual depths of $\geqslant$ 50 nm can be imaged by SEM techniques, especially if care is taken in selecting the operating conditions (e.g. [19, 24]). With conventional W- or LaB_6-sourced instruments, indentations with depths much smaller than this are difficult to resolve. Microstructural observations can be invaluable in investigating the deformation associated with the indentation process. Fig. 5a shows a typical 100 mN indentation from the normalized sample. Of the 50 indentations imaged, only one showed any evidence of obvious cracking near the indentation. Further, all the indentations were clearly delineated. By contrast, Fig. 5b shows a 100 mN indentation from the water-quenched sample. In this case, the indentation is less clearly delineated (i.e. the outline is less sharply imaged) and there is obvious "pin-cushioning" of the indentation outline (see Section 4.3).

3.5. Creep experiments

The creep behaviour of materials using nanoindentation techniques has previously been analysed by two different methods. The first of these uses a high-load hold segment where the load is maintained at a constant value. This is then compared to a lower load hold segment which is used to subtract any thermal drift from the data (e.g. [22]). The second approach has been to use an alternating force (a.c.) technique (e.g. [23]) which uses the superposition of a very small low-frequency a.c. signal on to the load coil of the indentor [25]. The phase and amplitude of the resultant response can then be compared with the original phase and amplitude of the load coil to obtain

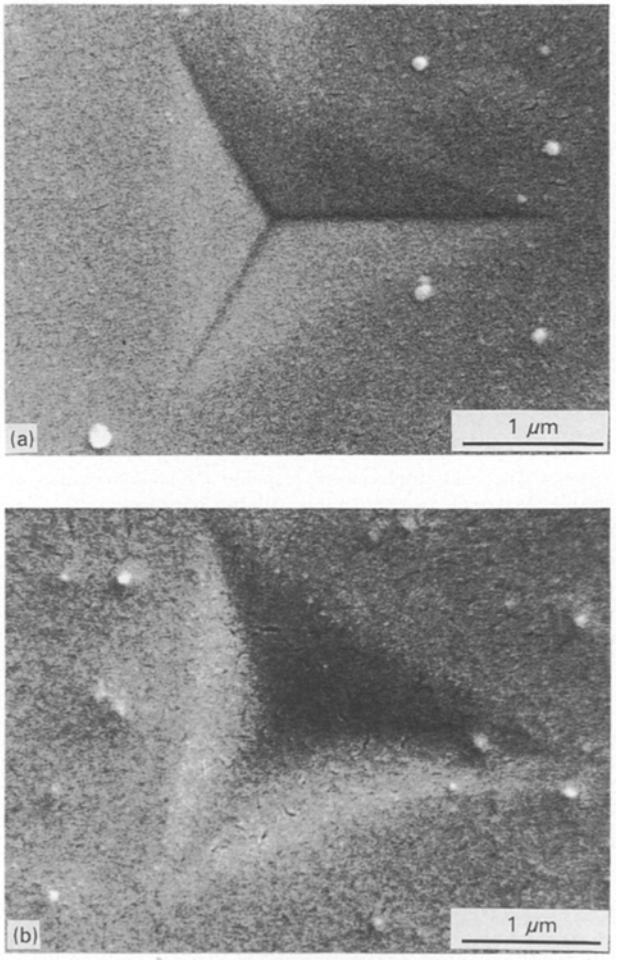

Figure 5 Scanning electron micrographs (15 kV, secondary electron images) of 100 mN indentations in (a) the normalized sample and (b) the water-quenched sample. The load–displacement curves for the particular indentations are near-identical but the appearance of the indentations is obviously dissimilar. (a) A sharply delineated plastic indentation outline; (b) is far less distinct despite the surface detail being sharply imaged. This suggests that considerable near-surface elastic recovery has occurred in (b) which is supported by the marked pin-cushion shape. Neither indentation shows any evidence of extrusion of any thin soft layer or contact-induced cracking in, or around, the indentation (see text).

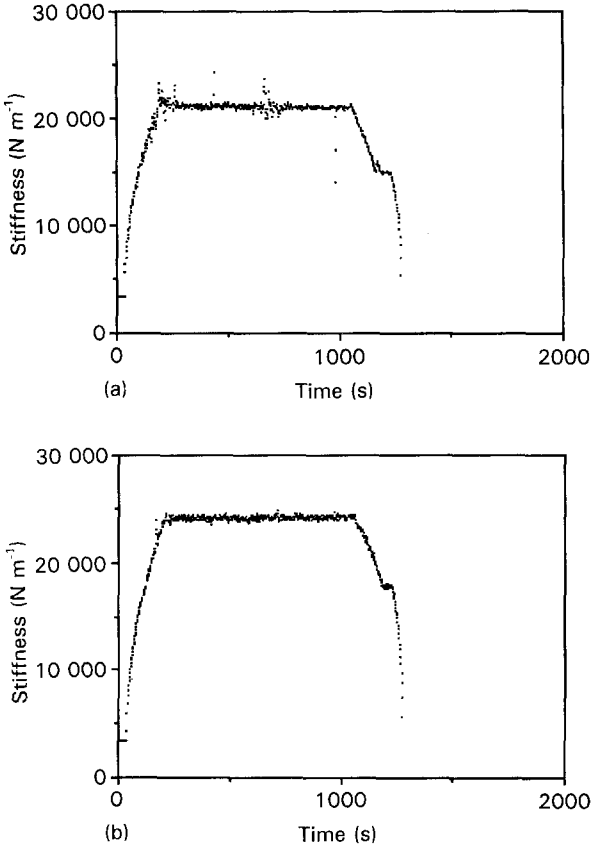

Figure 6 Typical contact stiffness versus time plots which were used to investigate indentation creep behaviour. Creep would be apparent as an increase in stiffness (at constant load) with time as the plastic contact area increases. No apparent effect was detected even at time scales (1000 s) commensurate with those claimed to show significant creep effects in low load microhardness tests (see text).

the stiffness of the contact and thus the sample. There are two advantages to this method, the first being that the stiffness is continuously monitored and therefore thermal drift effects are minimized, while the second is that the stiffness is monitored without needing to know the area of contact between the tip and the sample, and therefore the creep behaviour of very small indentations can be studied. This approach has been used to study the time-dependent deformation of a normalized and a water-quenched sample. The resultant stiffness versus time plots are shown in Fig. 6. The creep rate is obtained by fitting a curve to the stiffness versus time data for the long hold period. It can be seen from the curves that the slope of the two plots for the hold segment is virtually horizontal for both of the samples (this was confirmed by comparing the raw data at the beginning and end of this segment). This shows that there is effectively no creep occurring because any time-dependent change in the area of contact would significantly increase the stiffness. This is in contrast to previously reported results where anomalous indentation creep effects have been clearly demonstrated with large changes in contact area occurring over short times (~ 100 s) for the microhardness range.

4. Discussion

Conventional microhardness techniques for exploring chemomechanical effects have usually involved performing indentations through a continuous liquid film. At the outset, it is obvious that significant differences exist between this and our approach, (currently constrained by the nanoindentation technique itself) of using samples quenched into liquid and then tested dry. This has precluded us from observing any effects requiring either replenishment of liquid layers underneath the indentor or a high constant activity of species from the liquid which may be necessary to observe effects such as anomalous indentation creep. The differences are further accentuated by our specimen preparation procedure whereby, after drying, our samples have had to be heated to $\sim 60\,^{\circ}C$ to enable them to be rigidly waxed to the nanoindentor mounts. This may have promoted further desorption of any remnant physisorbed and chemisorbed species remaining from the liquids. Even so, nanoindentation has proved capable of identifying subtle but statistically significant differences in elastic and plastic behaviour which could not be observed by simple microhardness testing.

It could be argued that the technique of quenching, which has been widely used by a number of workers in the past (and is generally accepted as providing intimate substrate–liquid contact), may itself result in the subtle differences observed (for example, from differences in rates of heat transfer in different liquids) by either the generation of near-surface residual stresses or macro- or micro-cracking. However, even though residual stresses are known to affect indentation behaviour [26], simple calculations suggest that there should not be major differences between the samples here due to the differing quench environments. Some cracking of the sample surfaces was observed and it is likely that any residual stresses were relieved by these cracks. Further, care was taken to locate indentation arrays well away from obvious cracks. The observation that indentation behaviour changes significantly over a 4 week period of exposure to the ambient atmosphere suggests that it is the environment that is controlling many of these changes rather than any residual stresses or cracks whose effect would be expected to be more permanent. Also, Fig. 5 shows that there are no contact-induced cracks, in or around, the indentations.

4.1. Soft surface layers

Virtually all the samples appeared to display a mechanically soft surface layer, ~5 nm thick, which is presumed to be penetrated by the indentor before the expected response of the underlying sapphire is observed. As far as we know, this is the first direct mechanical observation of such a layer on a ceramic, though thin, water-softened layers have long been held responsible for many of the frictional properties of ceramics (e.g. [1]). The effect is quite reproducible and is similar in response to that reported for thin, soft gold films on silicon [27]. The load–displacement curve for a sample with no soft layer follows a smoothly parabolic shape (e.g. Fig. 7 for fused silica) whereas the curves with soft layers (e.g. Fig. 2a) show an initial flat portion followed by a distinct change in behaviour at ~5 nm where the curve rises steeply. The raw data curves for load and displacement were examined to check that this is not an instrumental artefact and a marked change in stiffness was always found to occur at the point taken to be the zero of our subsequent load–displacement plots.

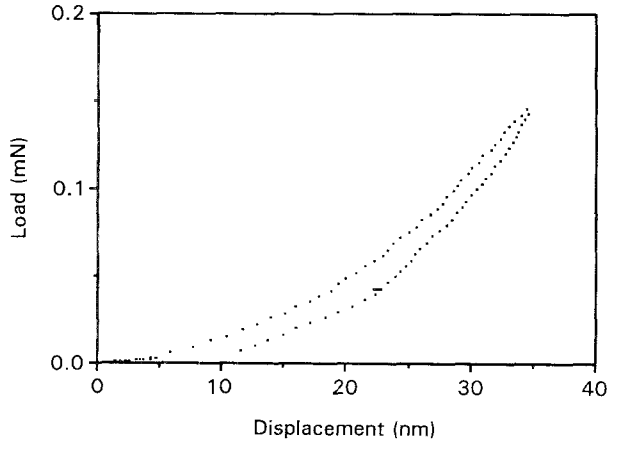

Figure 7 A typical load–displacement curve for a ~30 nm indentation in fused silica. The general curve is similar to Fig. 2b but no soft surface layer is detectable, demonstrating that the effect of a soft surface layer is not an instrumental artefact. (see text).

Interestingly, thin soft surface layers seem to be prevalent on most ceramic samples we have examined with the current exceptions of fused silica and some semiconductors (e.g. GaAs). For oxide ceramics, this effect is not surprising. For example, previous work by Bull and Page [1] showed (on MgO) that such thin, water-affected layers always seem to be present (as witnessed by their frictional response and infrared spectra) unless ion implantation had changed the near-surface charge distribution such that the driving force for charge neutralization by proton adsorption was removed. Thin soft layer effects are only seen at low loads as they only occur in the first few nanometres of the displacement and are therefore lost in load–displacement curves for larger indentations. These thin soft layers are certainly not detectable by microhardness experiments where much more substantial soft layers are required before differences in the hardness response can be observed (for example, the soft layers produced by amorphization during ion-implantation [28]).

4.2. Environmental effects on the elastic–plastic transition

Quenching identical samples into different environments creates subtle differences in the elastic–plastic transition (i.e. dislocation nucleation) and subsequent plastic flow. Firstly, 30 nm displacement indentations displayed either completely elastic behaviour (once the water-softened layer had been penetrated) or showed a response commensurate with plasticity having started at such small loads that the elastic–plastic transition itself could not be observed. In the latter cases, it is assumed that plastic flow is easily initiated by dislocation nucleation from stress-raising structural or chemical defects in the near surface (5–30 nm) layer. As the indentor displacement was moved to larger values (50 nm), copious pop-in behaviour was observed. Previously, this has been identified with dislocation nucleation in sapphire and it is possible to estimate the sub-surface shear stress generated by the indentor contact as plasticity is nucleated [19]. In all the cases reported here, pop-ins occurred at loads between 1 and 3 mN which, for the ~100 nm tip radius of the indentor used, corresponds to a maximum shear stress of $\sim E/50$, i.e. dislocation nucleation is occurring at approximately the theoretical strength and is thus presumed to be in good material beneath whatever soft layer and damage is on, or near, the surface.

For some of the samples, several pop-ins were seen on each of the curves. This is presumed to result from the need to nucleate dislocations at progressively deeper levels as the indentor penetrates into the surface. This may be affected by the crystallographic identity

and orientation of the slip systems activated (with respect to the indentor geometry and the sample surface) and also the ease with which slip nucleated from one source can accommodate plastic deformation at larger depths. Thus it is interesting that the $(10\bar{1}2)$ samples used here frequently showed multiple pop-ins while the (0001) samples in an earlier study [19] generally did not. The size of the pop-in displacement reflects both the number of dislocations created at each source and their Burgers vector [19] and thus it is difficult to use this as a Burgers vector diagnostic.

Following a 4 week exposure to moist laboratory air, virtually all samples showed dislocation pop-in at about the theoretical strength which suggests that the progressive adsorption and diffusion of water into the near-surface damaged layer eventually renders it structurally or mechanically impossible to propagate plastic flow from this layer into the underlying material. Two phenomena were observed to occur more frequently after long-term exposure to water. Firstly, more and smaller pop-ins occurred in each sample, and secondly, occasional pop-outs were seen. More frequent but smaller pop-ins suggest less dislocations were activated per source and thus more sources were necessary to accommodate the indentor displacement. In turn, this could reflect changes in either the source stress (source hardening) or the Peierls/friction stress for dislocation plasticity in sapphire [29, 30], i.e. either more difficult dislocation nucleation or less easy glide. Pop-out phenomena have previously been observed in single-crystal silicon (e.g. [19, 31]) where they are believed to be associated with the undensification of material compacted during loading. Thus, if any of the softened or damaged near-surface region was compacted on loading by the high hydrostatic component of the indentation stress field, then a similar undensification mechanism could account for the pop-outs seen here. Other explanations for the pop-out behaviour could include either a thin surface shell detaching itself from the bulk and trying to restore its unfixed position due to near-surface residual stresses (as may happen as a result of interfacial debonding with some residually compressed coatings [21]), or the collapse of a previously nucleated dislocation loops of subcritical size for stability. The latter again suggests possible changes in either dislocation source or friction stresses and in the absence of any evidence to the contrary, is the most likely and attractive explanation, given the presence of dislocation–nucleation causing pop-ins.

The changing balance between the combined effects of a thin soft layer (presumed to be either hydrated alumina [15] or a hydroxide layer), a thicker damaged layer and dislocation nucleation in a perfect crystal would explain anomalies in microhardness testing whereby some environments have been reported to cause softening and others hardening.

Unfortunately, we have no access to infra-red or other surface techniques which could definitely prove the long-term water adsorption hypothesis or chemically identify the adsorbates from the other environments, and this remains an obvious area for future work.

4.3. The appearance of nanoindentations

The SEM images in Fig. 5a and b show interesting differences even though at the (relatively high) 100 mN loads used to make the indentations, virtually no difference in the load–displacement response could be detected. Fig. 5a shows a typical indentation in the normalized sample with a sharply delineated indentation outline such as those commonly observed for many metals and ceramics. However, the indentation in the water-quenched sample (Fig. 5b) is less sharply delineated, despite being able to image sharply fine detail on the sample surface. Similar indistinct indentation outlines have previously been reported for coated systems (e.g. [21, 32]) where considerable elastic recovery in the hard coating leads to the residual indentation outline being less clearly defined than in those cases where the coating fractures and conforms to the underlying sub-surface plastically deformed impression in the substrate (e.g. Fig. 8). The appearance of Fig. 5b suggests that considerable near-surface elastic recovery is occurring which, in turn, implies that the majority of the plastic deformation is well below the surface. This is further supported by the marked pin-cushion appearance of the indentation which is usually associated with near-surface recovery of the indentation shape [19, 33, 34]. The previous observations are consistent with the interpretation of the pop-in (dislocation nucleation behaviour) occurring at larger (> 30 nm) indentor displacements in these samples.

Two further points arise from the micrographs in Fig. 5a and b. Firstly, neither of the indentations show any evidence consistent with the deformation (for example, extrusion from beneath the indentor) of a soft surface layer (cf. the behaviour of the thicker soft layer seen in Fig. 14 of [28]), although the contrast from this in the SEM would be weak because its dimensions (~ 5 nm) are small compared to the range of 10–30 kV beam electrons. Secondly, for all the

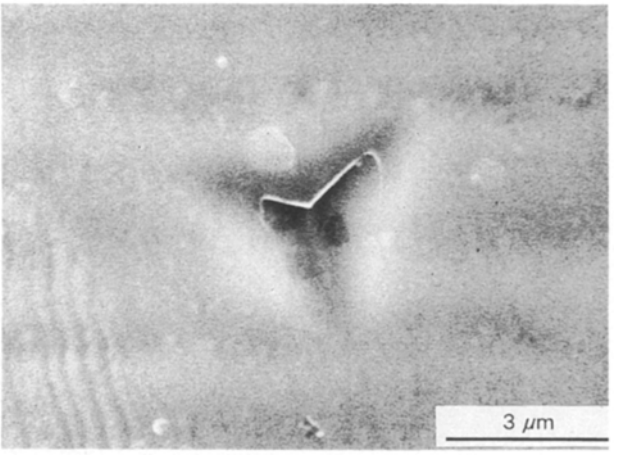

Figure 8 A 100 mN indentation in a coated sample (~ 0.5 μm of hard a:C–H on stainless steel) which, because of elastic recovery in the coating, appears indistinct except where the coating has cracked, allowing it to conform to the shape of the sub-surface plastic zone in the substrate. The appearance of this indentation should be compared with those shown in Fig. 5 (see text) (courtesy of T. Bartlett [32]).

samples (including the normalized and non-quenched sample) contrast consistent with myriads of small ($\sim$ 2–3 nm) surface markings can be observed. These markings could be from defects from the original polishing of the wafers or from the beginnings of thermal faceting during the anneal (similar to those observed in [19]). Their possible role in allowing environmental ingress of water/solvent into the surface and thus developing the soft surface layer is uncertain, and at these spatial resolutions, is difficult to determine further.

4.4. Nanoindentation and chemomechanical effects

It is immediately obvious from the above discussion that no single parameter such as hardness (either measured load-on or load-off), the maximum load for a given displacement, or the amount of elastic recovery gives a complete picture of the sample behaviour. In some cases individual parameters are approximately the same but the way in which the deformation occurred (for example, especially the position of pop-ins and pop-outs as witnessed on the load–displacement curve) is widely different. Thus, a number of parameters need to be calculated and the appearance of each load–displacement curve taken into account. A further advantage of nanoindentation is that the indentor displacement/penetration depth can be pre-set which allows like volumes of material to be examined. This is not the case with dead-loaded microhardness testing systems where, depending on the mechanical properties, the same load may be sampling effects in quite different sample volumes.

Given the very shallow indentations necessary to detect the differences in behaviour between environments, it has been impossible to make any reliable measurement of the sample stiffnesses (and therefore investigate possible changes in elastic moduli) and hardness values. Essentially this is because of the difficulties of accurately determining the exact tip-end geometry relevant to these small displacements. However, some possible changes in elastic properties could be influencing the differences in the $\%R$ behaviour measured here.

The observation that nanoindentation experiments in the load range which overlaps the microhardness range (e.g. 0.1 N) show no detectable differences in samples whose behaviour is clearly different at lower loads demonstrates the difficulty of using microhardness testing to explore chemomechanical effects. (Even higher load testing is precluded by long-term fluctuations in the displacement caused by even small amounts of heat transfer from the nanoindentor loading coil via the indentor shaft). However, it may be that under constant liquid films any changes are more pronounced and this would account for some of the reported differences in simple hardness behaviour when tested with much bigger loads than used here.

Although nanoindentation is an ideal way of exploring indentation creep behaviour, it was surprising that no significant rate of anomalous indentation creep was observed. The stiffness method that was employed is very sensitive to even small changes in contact area as any time-dependent plastic (or even elastic) deformation occurs. Thus it is concluded that anomalous indentation creep is probably only observed either at higher loads (i.e. a larger stressed sample volume) or under a continuous liquid film and therefore could, in large part, be due to lubrication effects of such films on the indenter. However, Burnett and Page [35] showed that ion-implanted ceramic surfaces displayed negligible indentation creep even under continuous liquid films and thus our observation may simply be either stress, or stressed volume limited.

Finally, the power and potential of nanoindentation techniques for exploring near-surface chemomechanical effects has been clearly demonstrated even though the methodology is not directly compatible with previous observations by ourselves and other workers in the area.

5. Conclusions

Nanoindentation techniques have been used to characterize the near-surface mechanical response of $(10\bar{1}2)$ single-crystal sapphire exposed to various environments thought to cause chemomechanical effects in ceramics. The specimens were annealed to desorb any physisorbed or chemisorbed species, then quenched into a number of liquid environments including water, ethanol, methanol and myristic acid and allowed to dry. The following conclusions can be drawn.

1. Significant differences in the near-surface mechanical properties have been revealed from the nanoindentation behaviour of single-crystal sapphire exposed to a range of environments.

2. A range of parameters need to be calculated from the load–displacement curves in order to reveal the differences in behaviour. Other phenomena (e.g. pop-in) are only evident from examination of the load–displacement curves themselves. No single parameter such as displacement at maximum load or hardness is sufficient to characterize the deformation behaviour.

3. Soft surface layers $\sim$5 nm thick were observed on virtually all the samples examined. This has been attributed to a layer directly affected by water adsorption.

4. Plastic flow was nucleated at either very low loads (presumed to be in a damaged near-surface layer < 30 nm thick) or, at larger displacements, by dislocation nucleation at approximately the theoretical strength (and presumed to be in good crystal).

5. After prolonged exposure to ambient laboratory atmosphere, virtually all the samples exhibited plasticity nucleation at the theoretical strength suggesting that the surface-damaged layer could no longer propagate plasticity into the bulk and thus had either been softened or otherwise modified by further water adsorption.

6. The number and size of pop-in events changed with time, suggesting subtle changes had occurred

affecting either dislocation source hardening or the Peierls/friction stress for subsequent dislocation glide.

7. The penetration resistance (as measured by the maximum load required to obtain a set displacement) of the samples varied, with the normalized sample initially being the highest and the water-quenched sample being the lowest. After prolonged exposure to ambient atmosphere, the penetration resistance of the samples changed and generally converged towards that of the original water-quenched sample.

8. Indentations to higher loads (100 mN – which overlaps with the conventional microhardness load range) showed no discernable differences in behaviour between samples which showed marked differences at lower loads.

9. Direct SEM observations of these larger (100 mN) indentations shows distinct differences in the near-surface appearance of the deformed surfaces establishing that more near-surface elastic recovery has occurred in the water-quenched sample (i.e. plastic deformation has occurred further from the surface in this case).

10. No evidence for anomalous indentation creep was observed even though previously this was the most widely reported chemomechanical effect at the microhardness scale. This suggests that either a larger stressed volume or the presence of liquid is required for creep to be observed.

11. High-resolution SEM observations reveal the existence of small ($\sim$2–3 nm) surface defects whose role in allowing environmental ingress is unclear but which might be responsible for the initial formation of the thin, markedly soft, near-surface layer.

12. The results presented clearly demonstrate the ability of nanoindentation to explore changes in the very near-surface mechanical properties of ceramics which are affected by phenomena such as chemomechanical effects. Further work is required in order to identify any adsorbed species and the various structural layers involved and to overcome the limitations of not being able to perform nanoindentation experiments through continuous liquid films.

Acknowledgements

The Materials Commission of the United Kingdom Science and Engineering Council are thanked for supporting the Newcastle Nano Indentor used for the experiments. S.V.H. would like to thank S.E.R.C., I.C.I. Fibres and Morgan Matroc Ltd, for financial support. Dr A. J. Whitehead, Mr P. Twigg, Mrs T. Bartlett and Mr G. Shore (final year M. Eng. undergraduate project) are thanked for their help and useful discussions. Mrs T. Bartlett is also thanked for the provision of Fig. 8.

References

1. S. J. BULL and T. F. PAGE, *J. Phys. D Appl Phys.* **22** (1989) 941.
2. T. E. FISCHER, *Ann. Rev. Mater. Sci.* **18** (1988) 303.
3. J. T. CZERNUSZKA and T. F. PAGE, *J. Microsc.* **140** (1985) 159.
4. T. SUGITA, K. UEDA and Y. KANEMURA, *Wear* **97** (1984) 1.
5. S. M. WEIDERHORN and H. JOHNSON, *J. Am. Ceram. Soc.* **58** (1975) 342.
6. A. R. C. WESTWOOD, N. H. MACMILLAN and R. S. KALYONCU, *J. Am. Ceram. Soc.* **56** (1973) 258.
7. N. H. MACMILLAN, R. D. H. HUNTINGTON and A. R. C. WESTWOOD, *J. Mater. Sci.* **9** (1974) 697.
8. A. R. C. WESTWOOD, J. S. AHEARN and J. J. MILLS, *Colloids Surfaces* **2** (1981) 1.
9. N. H. MACMILLAN, in "Surface Effects in Crystal Plasticity", edited by R. M. Latanision and J. T. Fourie (Noordhof Int., Leyden, 1977) p. 629.
10. P. B. HIRSCH, *J. Microsc.* **118** (1980) 3.
11. R. E. CUTHRELL, *J. Mater. Sci.* **14** (1979) 612.
12. J. H. WESTBROOK and P. J. JORGENSEN, *Trans AIME* **233** (1965) 425.
13. A. R. C. WESTWOOD and D. L. GOLDHEIM, *J. Appl. Phys.* **39** (1968) 3401.
14. W. W. WALKER, in "The Science of Hardness Testing and it's Research Applications", edited by J. H. Westbrook and J. Conrad (ASM, Metals Park, OH, 1973) pp. 258–73.
15. J. T. CZERNUSZKA and T. F. PAGE, *J. Mater. Sci.* **22** (1987) 3917.
16. J. B. PETHICA, R. HUTCHINGS and W. C. OLIVER, *Philos. Mag. A* **48** (1983) 593.
17. J. D. J. ROSS, H. M. POLLOCK, J. C. PIVIN and J. TAKADOUM, *Thin Solid Films* **148** (1987) 171.
18. M. F. DOERNER, D. S. GARDNER and W. D. NIX, *J. Mater. Res.* **1** (1986) 845.
19. T. F. PAGE, W. C. OLIVER and C. J. McHARGUE, *ibid.* **7** (1992) 450.
20. G. M. PHARR and W. C. OLIVER, *MRS Bull.* **17** (1992) 28.
21. T. F. PAGE and S. V. HAINSWORTH, *Surf. Coat. Technol. A* **61** (1993) 201.
22. S. P. BAKER, T. W. BARBEE Jr and W. D. NIX, *Mater. Res. Soc. Symp. Proc.* **239** (1992) 319.
23. T. P. WEIHS and J. B. PETHICA, *ibid.* **239** (1992) 325.
24. S. V. HAINSWORTH, PhD Thesis, University of Newcastle upon Tyne (1993).
25. J. B. PETHICA and W. C. OLIVER, *Mater. Res. Soc. Symp. Proc.* **130** (1989) 13.
26. J. C. KNIGHT, T. F. PAGE and I. M. HUTCHINGS, *Surf. Eng.* **5** (1989) 213.
27. A. J. WHITEHEAD and T. F. PAGE, *Thin Solid Films* **220** (1992) 277.
28. P. J. BURNETT and T. F. PAGE, *J. Mater. Sci.* **19** (1984) 3524.
29. B. T. KELLY, "Irradiation Damage to Solids" (Pergamon, Oxford, 1966) p. 140.
30. P. B. HIRSCH, "The Physics of Metals: Defects" (Cambridge University Press, Cambridge, 1975) p.182.
31. G. M. PHARR, *Mater. Res. Soc. Symp. Proc.* **239** (1992) 301.
32. T. WRIGHT and T. F. PAGE, *Surf. Coat. Technol.* **54/55** (1992) 557.
33. P. M. SARGENT and T. F. PAGE, *J. Mater. Sci.* **20** (1985) 2388.
34. D. TABOR, "Hardness of Metals" (Clarendon Press, Oxford, 1951).
35. P. J. BURNETT and T. F. PAGE, *J. Mater. Sci. Lett.* **4** (1985) 1364.

Received 11 April
and accepted 19 April 1994